



Matrix effects and their role in the low-temperature photochemistry of $(\eta\text{-Aniline})\text{Cr}(\text{CO})_3$

Mohammed H. Alamiry, Conor Long*, Padraig P. Fidgeon, Mary T. Pryce

School of Chemical Sciences, Dublin City University, Dublin 9, Ireland

ARTICLE INFO

Article history:

Received 17 February 2010

Received in revised form

12 April 2010

Accepted 15 April 2010

Available online 24 April 2010

Keywords:

Chromium

Carbonyl

Aniline

Matrix isolation

Photochemistry

ABSTRACT

The low-temperature chemistry and photochemistry of $(\eta^6\text{-Aniline})\text{Cr}(\text{CO})_3$ was investigated by matrix isolation techniques in frozen CH_4 or N_2 . The spectroscopic properties of the matrix changed both during the deposition process and also following annealing of the matrix to 40 K. These changes are explained by the elimination of lattice defects in the crystalline medium which forces haptotropic changes to $(\eta^6\text{-Aniline})\text{Cr}(\text{CO})_3$ producing $(\eta^2\text{-N-Aniline})\text{Cr}(\text{CO})_3$ and $(\eta^3\text{-N-Aniline})\text{Cr}(\text{CO})_3$ as identified by IR spectroscopy. These assignments are supported by DFT calculations which also provide estimates of the energetics of the haptotropic shift processes. The reduced hapticity species exhibit different photochemical properties compared to $(\eta^6\text{-Aniline})\text{Cr}(\text{CO})_3$. They undergo complete decarbonylation following irradiation at 436 nm.

© 2010 Elsevier B.V. All rights reserved.

1. Introduction

The high quantum yields of photo-induced CO-loss from metal carbonyl compounds has resulted in their status as prototypical systems for many time resolved and low temperature photochemical techniques [1]. For instance the photo-induced CO-loss from $\text{Cr}(\text{CO})_6$ has been the subject of numerous experimental studies from the early days of flash photolysis [1–10] and matrix isolation [11–13], to modern ultrafast non-resonant techniques [14]. These studies are now supported by sophisticated excited state calculations which explain the excited state dynamics preceding CO-loss [15,16]. Frequently photo-induced CO-loss involves nuclear motion along a highly accelerating potential energy surface producing product fragments on the timescale of molecular vibrations (< 100 fs) and with non-statistical energy distributions [14,17–23]. However not all photo-induced CO-loss occurs on the sub-ps timescale [24]. Our recent work on $(\eta^6\text{-Benzene})\text{Cr}(\text{CO})_3$ showed that CO-loss occurs on a timescale three orders of magnitude slower than from the homolyptic $\text{Cr}(\text{CO})_6$ complex [25]. Indeed it is possible that the behaviour observed for homolyptic complexes may not be typical of the less symmetric heterolyptic systems.

We have also reported a significant difference between the photochemical behaviour of $(\eta^6\text{-Benzene})\text{Cr}(\text{CO})_3$ in room temperature solution when compared to low temperature frozen gas matrixes [26]. In room temperature *n*-heptane solution, photolysis at 400 nm depleted the ν_{CO} bands of $(\eta^6\text{-Benzene})\text{Cr}(\text{CO})_3$ and produced ν_{CO} bands of an excited state species $[(\eta^6\text{-Benzene})\text{Cr}(\text{CO})_3]^*$ which ejects CO over 150 ps to produce $(\eta^6\text{-Benzene})\text{Cr}(\text{CO})_2$. In contrast, irradiation of $(\eta^6\text{-Benzene})\text{Cr}(\text{CO})_3$ at 405 nm in a methane matrix at 12 K resulted in the bleaching of its ν_{CO} bands but with no significant product band formation (apart from uncoordinated CO). Failure to observe $(\eta^6\text{-Benzene})\text{Cr}(\text{CO})_2$ formation at 12 K was explained by proposing the existence of a small thermal barrier to CO-loss from the $[(\eta^6\text{-Benzene})\text{Cr}(\text{CO})_3]^*$ excited state species which could not be surmounted at 12 K following 405 nm irradiation [25]. However no explanation was available for the lack of photoproduct ν_{CO} bands despite the substantial depletion of $(\eta^6\text{-Benzene})\text{Cr}(\text{CO})_3$ in these experiments [26].

Recently the photochemistry of a series of $(\eta^6\text{-Arene})\text{Cr}(\text{CO})_3$ and $(\eta^5\text{-Cp})\text{Mn}(\text{CO})_3$ (Cp = cyclopentadienyl) complexes containing tethered donor atoms (e.g. sulphur or nitrogen) on the cyclic ligand have been investigated by Heilweil, Burkey and co-workers [27,28]. This work demonstrated the potential for using such systems as photochromic devices where the coordination mode of the ligand could be altered following photoejection of a CO ligand, with concomitant changes to the absorption characteristics of both the UV/vis. and IR spectra. In addition, quantum chemical calculations

* Corresponding author. Tel.: +353 1 7008001; fax: +353 1 7005503.
E-mail address: conor.long@dcu.ie (C. Long).

by Weitz et al. on $(\eta^6\text{-Benzene})\text{Cr}(\text{CO})_3$ located a reduced hapticity species ($\eta^1\text{-C-Benzene})\text{Cr}(\text{CO})_3$ at a minimum on the singlet hypersurface. This introduces the possibility that such reduced hapticity species may play a part in the photochemistry of $(\eta\text{-Benzene})\text{Cr}(\text{CO})_3$ at low temperatures under appropriate conditions [29].

These results have prompted us to investigate the behaviour of $(\eta^6\text{-Aniline})\text{Cr}(\text{CO})_3$ in low temperature matrixes, principally CH_4 . The long-held assumption that the structure of an organometallic complex is unaffected by the matrix isolation technique appears not to hold for these systems. We report evidence that changes to the spectroscopic and photochemical properties of the isolated material can occur during the deposition process and also upon annealing the matrix. These changes are the result of alterations to the coordination mode of the aniline ligand with respect to the $\text{Cr}(\text{CO})_3$ unit. DFT methods were used to identify reduced hapticity species and to estimate the thermal barriers to their formation from $(\eta^6\text{-Aniline})\text{Cr}(\text{CO})_3$ in the gas phase. These calculations suggest that the formation of the reduced hapticity species requires the surmounting of a considerable energy barrier far in excess of that available in the matrix isolation experiments. We propose that the reduction in defect concentrations during matrix annealing dominates the Gibbs free energy change of the process forcing the haptotropic shift process of the isolated material. Thus the formation of a rigid lattice surrounding $(\eta\text{-Aniline})\text{Cr}(\text{CO})_3$, constrains the molecule to adopt a structure not easily accessible in the fluid phase. This can facilitate the study of unusual coordination isomers of some organometallic complexes which can then be examined using photochemical techniques.

2. Results

2.1. Low temperature matrix isolation

The spectroscopic changes which occur during the deposition of $(\eta^6\text{-Aniline})\text{Cr}(\text{CO})_3$ in a CH_4 matrix were initially monitored by UV/vis. spectroscopy and are presented in Fig. 1 (these spectra are normalized to exhibit the same absorbance at 312 nm to facilitate band-shape comparisons). During the course of the deposition, the absorption feature at 312 nm broadens and extends further into the visible region. The deposition was also monitored using IR spectroscopy which, for technical reasons, involved separate experiments. The spectral changes are presented in Fig. 2 and were normalized at 1894 cm^{-1} . These show an increasing absorbance at approximately 1960 cm^{-1} along with a broad feature centred at 1870 cm^{-1} . More pronounced changes occur when the matrix

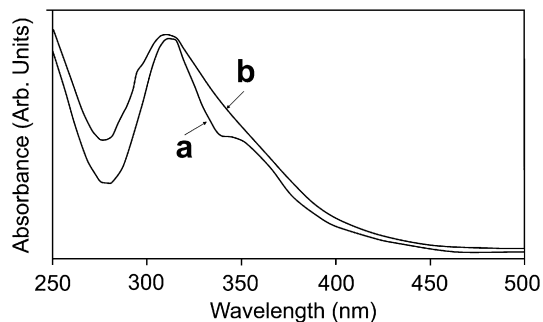


Fig. 1. The normalized (at 312 nm) UV/vis. spectra obtained during the deposition of $(\eta^6\text{-Aniline})\text{Cr}(\text{CO})_3$ in a CH_4 matrix at 20 K. The spectra were measured following (a) 15 and (b) 170 minutes deposition from a sample held at 325 K. For clarity an offset of +0.01 AU has been applied to spectrum (b), the absorption broadens as the deposition progresses.

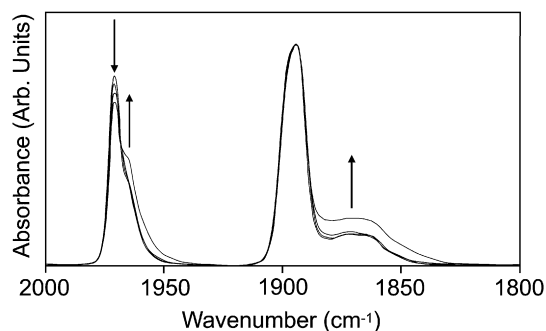


Fig. 2. The IR spectral changes observed during the deposition of $(\eta^6\text{-Aniline})\text{Cr}(\text{CO})_3$ in a CH_4 matrix. Spectra were obtained during deposition at 60, 120, 180 and 240 minutes. The spectra were normalized at 1894 cm^{-1} . Arrows represent the change in relative absorbance of features showing the increased formation of haptotropic shift species as the deposition progresses.

temperature was allowed to increase to 30, 35 and finally to 40 K (matrix annealing) as presented in Fig. 3(a). The changes are explained by the production of haptotropic shift species, either $(\eta^2\text{-N-Aniline})\text{Cr}(\text{CO})_3$ or $(\eta^3\text{-N-Aniline})\text{Cr}(\text{CO})_3$. This conclusion is supported by the results of quantum chemical calculations outlined below. Thus it would appear that the species responsible for the bands at 1961, 1881, and 1864 cm^{-1} are also responsible for the broadening of the UV/vis. absorption band. Similar spectroscopic changes occurred upon annealing a N_2 matrix containing $(\eta^6\text{-Aniline})\text{Cr}(\text{CO})_3$ (Fig. 3(b)). Solid N_2 (m.p. 63 K) has a hexagonal close packed structure with a phase transition to a cubic structure at 35 K.

The IR changes observed following irradiation of a CH_4 matrix containing $(\eta^6\text{-Aniline})\text{Cr}(\text{CO})_3$ is presented in Fig. 4. Spectrum (a) in this figure is a difference spectrum obtained by subtracting the spectrum of the pre-irradiated non-annealed matrix from the spectrum of the matrix following irradiation with $\lambda_{\text{exc.}} > 320\text{ nm}$. The depletion of $(\eta^6\text{-Aniline})\text{Cr}(\text{CO})_3$ is confirmed by the negative

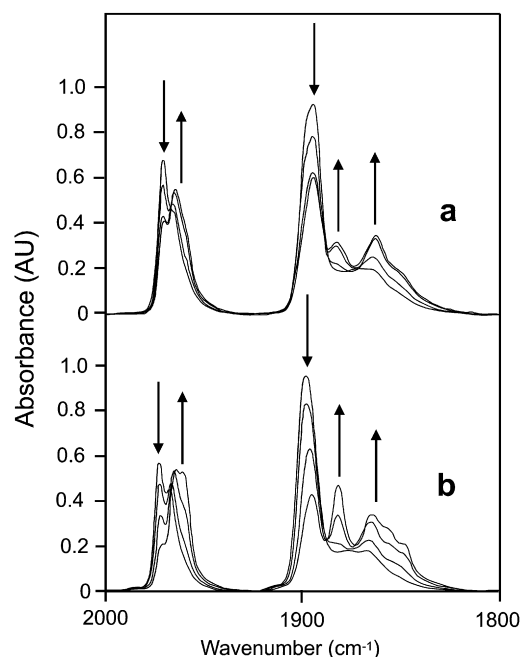


Fig. 3. The IR spectral changes observed upon annealing a CH_4 matrix containing $(\eta^6\text{-Aniline})\text{Cr}(\text{CO})_3$; spectra were obtained at 20, 30, 35 and 40 K showing the growth of bands at 1964, 1961, 1881, and 1864 cm^{-1} . Other features were observed as shoulders on the low energy side of the 1864 cm^{-1} band.

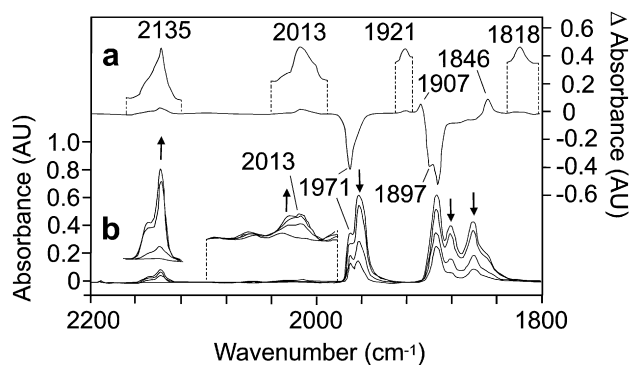


Fig. 4. (a) The spectral changes observed following broad-band irradiation (>320 nm) of a non-annealed CH₄ matrix (difference spectrum) containing (η^6 -Aniline)Cr(CO)₃ showing depletion of the parent bands (negative) and production of uncoordinated CO (3135 cm⁻¹) and bands for (η^6 -Aniline)Cr(CO)₂(CH₄) (1907 and 1846 cm⁻¹) and weak features at 2013, 1921, and 1818 cm⁻¹. (b) shows the spectral changes observed following monochromatic irradiation (436 nm) of an annealed CH₄ matrix containing (η^6 -Aniline)Cr(CO)₃ species showing preferential depletion of the reduced hapticity species, formation of uncoordinated CO and a weak feature at 2013 cm⁻¹.

peaks at 1898 and 1971 cm⁻¹. Photoproduct bands are evident at 1846 and 1907 cm⁻¹ assigned to (η^6 -Aniline)Cr(CO)₂(CH₄) as observed previously [26]. In addition, a broad asymmetric feature in the region where uncoordinated CO absorbs (circa 2135 cm⁻¹) confirms the photo-induced decarbonylation of (η^6 -Aniline)Cr(CO)₃. The shape of this band suggests that the CO is produced in a variety of environments. Some may interact with the metal fragment or other CO molecules. Carbon monoxide dimers have been observed in argon matrices (2140.1 cm⁻¹) at higher energy compared to monomeric CO (2138.5 cm⁻¹) [30]. Two Voigt functions are sufficient to model this feature; with centers at 2138 and 2148 cm⁻¹ [31]. The ratio of the areas of the Voigt (amplitude Gaussian/Lorentian) functions remained constant at 1.23:1 throughout the irradiation suggesting that both features are produced in a coordinated process. In addition to these bands further very weak features are also evident at 1818, 1921, and 2013 cm⁻¹. Unfortunately because these features are weak it was not possible to determine if they arise from a single or multiple product species. Subsequent monochromatic irradiation of an annealed matrix as described below, suggest that at least two species are implicated in producing these bands.

Fig. 4(b) presents a series of spectra obtained following irradiation of an annealed matrix (matrix temperature brought to 35 K and then returned to 20 K) using 436 nm light. It is important to note that 436 nm is approaching the lower limit of the absorption profile of (η^6 -Aniline)Cr(CO)₃ complexes (Fig. 1). However calculations, described below, indicate that the reduced hapticity species (η^3 -Aniline)Cr(CO)₃ or (η^2 -Aniline)Cr(CO)₃ have higher extinctions at 436 nm than does (η^6 -Aniline)Cr(CO)₃. It is clear from these spectra that the spectral features of reduced hapticity species (1962, 1880, and 1860 cm⁻¹) suffer a greater depletion under these irradiation conditions than do the features of (η^6 -Aniline)Cr(CO)₃ (1971, 1897, and 1894 cm⁻¹). Thus the reduced hapticity species are preferentially excited. Apart from uncoordinated CO the only product band observed in these experiments occurs as a very weak feature at 2013 cm⁻¹. There is no evidence for bands at 1921 or 1818 cm⁻¹ which suggests that the three bands observed in Fig. 4 (a) (1818, 1921, and 2013 cm⁻¹) are the result of at least two metal carbonyl photoproducts. The feature in the uncoordinated CO region is asymmetric and consists of two partially resolved bands similar to that observed in Fig. 4(a).

In an attempt to trap possible metal carbonyl intermediates the photolysis experiment was repeated using N₂ as the isolating

matrix. There are many examples where coordinatively unsaturated intermediates react with the “active” matrix gases N₂ to form M–N₂ complexes following photolysis. These can then be detected by their ν_{NN} bands [32]. The deposition of this matrix was monitored by both UV/vis. and IR spectroscopy and the temperature was maintained at 20 K. The bands of (η^6 -Aniline)Cr(CO)₃ species were observed at 1864, (sh), 1877 (sh), 1898, 1967, and 1972 cm⁻¹. Exhaustive irradiation (> 10 hours 250 W Ar/Hg lamp) of this matrix at 405 nm resulted in almost complete depletion (> 90%) of the ν_{CO} bands of the (η^6 -Aniline)Cr(CO)₃ without the formation of M–CO or M–N₂ fragments. This degree of depletion of the ν_{CO} bands when a metal carbonyl complex is irradiated in low temperature matrices is very unusual particularly at such a low irradiation energy. Typically, the UV/vis. absorption of the CO-loss species occur at lower energies compared to their parent species [33,34], and irradiation at a specific wavelength is expected to result in the build up to steady-state concentrations of both parent complex and photoproduct(s).

A further experiment was conducted using a CH₄ matrix doped with CO to a level of 10% (v/v). Again irradiation at 405 nm resulted in depletion of the bands of (η^6 -Aniline)Cr(CO)₃ however no M–CO intermediates were detected. However reducing the irradiation wavelength to 334 nm produced IR features consistent with the formation of (η^6 -Aniline)Cr(CO)₂(CH₄). Thus following irradiation at 334 nm a single CO is ejected from (η^6 -Aniline)Cr(CO)₃ and this process occurs from a higher energy excited state than that populated by 405 nm irradiation. These experiments confirm that some photochemical route to the destruction of (η^6 -Aniline)Cr(CO)₃ exists following irradiation at 405 nm but that this process does not produce a detectable metal carbonyl products under steady-state irradiation at low temperature.

2.2. Computational studies

Molecular mechanics calculations provided a starting structure of (η^6 -Aniline)Cr(CO)₃ for a subsequent structural optimisation to tight convergence limits. The DFT calculations were performed at the B3LYP/LANL2DZp level, a reasonable compromise between accuracy and computational cost [25,26,35]. The LANL2DZ double ζ basis set was augmented with an f-function on the chromium atom (LANL2DZp) [36]. Selected structural parameters of the optimized structure obtained from these calculations are presented in Table 1. Calculation of the force constants and resulting vibrational frequencies confirmed that the optimized structure was located at a minimum on the potential energy hypersurface. The calculated ν_{CO} band positions were multiplied by a correction factor of 1.018, derived by equating the calculated vibrational frequencies of the ν_{CO} bands with those observed for (η^6 -Aniline)Cr(CO)₃ in a CH₄

Table 1

The calculated Mulliken charges on the chromium atom of the various singlet complexes in this study along with selected bond lengths in Å.

Complex	Mulliken Charge on Cr (C)	Cr–C1 Distance in Å	Cr–C2	C4–N	Cr–CO ^a	CrC–O ^a
(η^6 -Aniline)Cr(CO) ₃	-0.160	2.44608	2.35048	3.52736	1.82746	1.18986
(η^3 -N-Aniline)Cr(CO) ₃	0.063	2.38934	2.49818	2.16682	1.81527	1.19408
(η^2 -N-Aniline)Cr(CO) ₃	0.045	2.23566	2.78097	2.20071	1.81700	1.19365
(η^1 -Cl-Aniline)Cr(CO) ₃ TS ^b	-0.013	2.32834	2.55740 ^c	2.90835	1.81287	1.19282

^a An average of the three bond lengths.

^b The transition state between the η^6 and η^2 -N species.

^c Average of two bond lengths.

Table 2

The observed and calculated IR spectroscopic parameters for the complexes in this study.

Compound		ν_{CO}			
$(\eta^6\text{-Aniline})\text{Cr}(\text{CO})_3$	Singlet	1894	1897	1971	Observed
$(\eta^2\text{-N-Aniline})\text{Cr}(\text{CO})_3$	Singlet	1867	1876	1958	Calculated
$(\eta^3\text{-N-Aniline})\text{Cr}(\text{CO})_3$	Singlet	1864	1875	1957	Calculated
$(\eta^2\text{-N-Aniline})\text{Cr}(\text{CO})_3$	Triplet	1990	2018	2078	Calculated
$(\eta^6\text{-Aniline})\text{Cr}(\text{CO})_3$	Triplet	1862	1899	1965	Calculated

matrix at 20 K (Table 2). This correction factor is similar to those used in other studies on related complexes [25,35,37]. The excited state energy of the 20 lowest energy spin allowed transitions was obtained from Time-Dependent DFT (TDDFT) calculations. These data are presented in Table 3.

A relaxed potential energy scan was undertaken to investigate other possible coordination modes for the aniline ligand. In these calculations the distance between the chromium and the nitrogen atom was reduced from 3.5273 Å (the calculated Cr–N distance in the optimized structure of $(\eta^6\text{-Aniline})\text{Cr}(\text{CO})_3$) to 2.0273 Å in steps of 0.1 Å. At each step all other structural parameters were

Table 3

Vertical excitation energies obtained from TDDFT calculations for the lowest energy spin allowed transitions of $(\eta^6\text{-Aniline})\text{Cr}(\text{CO})_3$, $(\eta^2\text{-N-Aniline})\text{Cr}(\text{CO})_3$ and ${}^3(\eta^4\text{-N-Aniline})\text{Cr}(\text{CO})_3$, only transitions with an oscillator (osc.) strength (in parenthesis) greater than 0.0001 are presented. The data are presented to demonstrate how the allowed absorptions for $(\eta^2\text{-N-Aniline})\text{Cr}(\text{CO})_3$ and ${}^3(\eta^4\text{-N-Aniline})\text{Cr}(\text{CO})_3$ extend towards the red end of the visible spectrum.

$(\eta^6\text{-Aniline})\text{Cr}(\text{CO})_3$	$(\eta^2\text{-N-Aniline})\text{Cr}(\text{CO})_3$	${}^3(\eta^4\text{-N-Aniline})\text{Cr}(\text{CO})_3$
singlet	Singlet	triplet
nm (osc. strength)	nm (osc. strength)	nm (osc. strength)
		2218.23 (0.0007)
		864.46 (0.0010)
		796.18 (0.0008)
	729.98 (0.0008)	
	695.85 (0.0053)	
	638.24 (0.0088)	
		601.38 (0.0002)
		531.38 (0.0020)
	495.72 (0.0022)	
	467.69 (0.0093)	
		466.17 (0.0017)
		440.07 (0.0009)
	434.34 (0.0260)	
		430.64 (0.0008)
		407.56 (0.0021)
		401.36 (0.0002)
		398.78 (0.0004)
396.13 (0.0003)		
388.99 (0.0018)		
370.50 (0.0018)		374.22 (0.0066)
367.23 (0.0042)		367.71 (0.0021)
	365.91 (0.0018)	
	365.89 (0.0040)	
		361.55 (0.0037)
357.86 (0.0003)		
352.48 (0.0137)	348.50 (0.0029)	352.03 (0.0006)
	346.57 (0.0027)	344.63 (0.0014)
338.29 (0.0013)	333.58 (0.1126)	
327.55 (0.0014)		323.67 (0.0291)
		319.54 (0.0093)
316.25 (0.0106)		315.19 (0.0096)
311.19 (0.0015)		
305.87 (0.0008)		
295.14 (0.1263)		
280.27 (0.0006)	282.70 (0.0132)	
275.03 (0.0030)	278.56 (0.0019)	
272.84 (0.0023)	274.02 (0.0101)	
267.77 (0.0170)		
	263.46 (0.0016)	
258.09 (0.0003)		
256.66 (0.0001)		

optimized. An *exo*-cyclic coordinated species ($(\eta^3\text{-N-Aniline})\text{Cr}(\text{CO})_3$) was located in these calculations (Fig. 5(a)). Selected structural parameters and Mulliken charges on the chromium atom are presented in Table 1 and these indicated a reduction in electron density on the chromium atom in the reduced hapticity complexes. It should be noted that the transformation from $(\eta^6\text{-Aniline})\text{Cr}(\text{CO})_3$ to $(\eta^3\text{-N-Aniline})\text{Cr}(\text{CO})_3$ also involved a rotation of the Cr(CO)₃ fragment relative to the aniline ligand as indicated in Fig. 6. A synchronous transit-guided quasi-Newton method was used to locate a transition state between the optimized structures of $(\eta^3\text{-N-Aniline})\text{Cr}(\text{CO})_3$ and $(\eta^6\text{-Aniline})\text{Cr}(\text{CO})_3$. This transition state (TS) species exhibited a structure close to that of a $(\eta^1\text{-C1-Aniline})\text{Cr}(\text{CO})_3$ species, labelled $(\eta^1\text{-C1-Aniline})\text{Cr}(\text{CO})_3\text{TS}$ in Table 1. Examination of the Hessian matrix indicated the presence of only one negative eigenvalue (-149 cm^{-1}) which confirms that $(\eta^1\text{-C1-Aniline})\text{Cr}(\text{CO})_3\text{TS}$ is indeed a transition state on the potential energy hypersurface.

An extensive reaction path mapping was undertaken using $(\eta^1\text{-C1-Aniline})\text{Cr}(\text{CO})_3\text{TS}$ as the starting structure and following the single imaginary mode in both the forward and reverse directions. This reaction path joined an $(\eta^6\text{-Aniline})\text{Cr}(\text{CO})_3$ species with $(\eta^2\text{-N-Aniline})\text{Cr}(\text{CO})_3$. The $(\eta^2\text{-N-Aniline})\text{Cr}(\text{CO})_3$ species has a slightly lower energy (6 kJ mol^{-1}) than the $(\eta^3\text{-N-Aniline})\text{Cr}(\text{CO})_3$ species described above. An estimate of the activation energy (79 kJ mol^{-1}) for the $(\eta^6\text{-Aniline})\text{Cr}(\text{CO})_3$ to $(\eta^2\text{-N-Aniline})\text{Cr}(\text{CO})_3$ haptotropic shift was obtained from these calculations. It should be noted that the structure of the $(\eta^6\text{-Aniline})\text{Cr}(\text{CO})_3$ species derived from the reaction path modelling was not the same as that obtained from the structure optimisation calculations on $(\eta^6\text{-Aniline})\text{Cr}(\text{CO})_3$. The optimized structure of $(\eta^6\text{-Aniline})\text{Cr}(\text{CO})_3$ has an eclipsed-N conformation where the carbonyl group eclipses the arene carbon bonded to the amine substituent (Fig. 7). The terminal structure obtained from the reaction path modelling calculations has an eclipsed-C conformation, where the carbonyl groups eclipse the un-substituted arene carbons.

A relaxed potential energy scan on the $(\eta^6\text{-Aniline})\text{Cr}(\text{CO})_3$ species where the Cr(CO)₃ fragment was rotated relative to the aniline ligand provided an estimate of the rotational barrier to the eclipsed-N to eclipsed-C conformation of approximately 12 kJ mol^{-1} . This barrier while small, is significantly larger than that calculated for $(\eta^6\text{-Benzene})\text{Cr}(\text{CO})_3$ ($2\text{--}3\text{ kJ mol}^{-1}$) [38]. However it

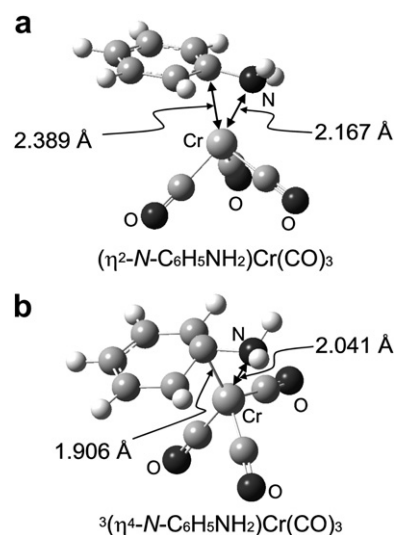


Fig. 5. The optimized structures of (a) $(\eta^3\text{-N-Aniline})\text{Cr}(\text{CO})_3$ and (b) ${}^3(\eta^4\text{-N-Aniline})\text{Cr}(\text{CO})_3$. Bond lengths of the Cr–N and Cr–C1 atoms are provided.

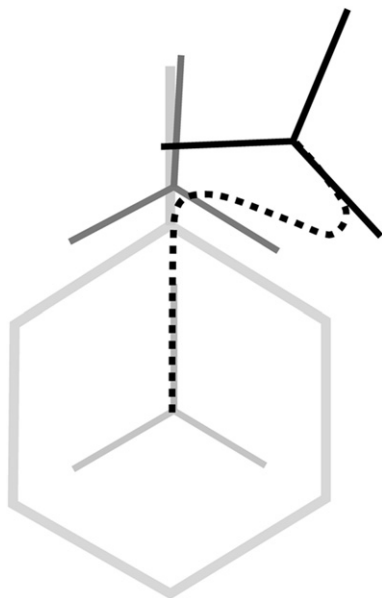


Fig. 6. The rotation of the $\text{Cr}(\text{CO})_3$ fragment (represented by progressively darker three pointed star) relative to the aniline ligand during the relaxed potential energy scan involving altering the Cr to N distance from 3.5273 Å in $(\eta^6\text{-Aniline})\text{Cr}(\text{CO})_3$ to 2.0273 Å in steps of 0.1 Å. The dashed curve represents the motion of the chromium atom

is consistent with structural and spectroscopic studies on systems containing electron donating substituents such as amine groups on the arene ligand where the eclipsed-*N* configuration is favoured [39–41].

The optimized structures of both $(\eta^2\text{-}N\text{-Aniline})\text{Cr}(\text{CO})_3$ and $(\eta^3\text{-}N\text{-Aniline})\text{Cr}(\text{CO})_3$ were used to locate a transition state ($(\eta^3\text{-}N\text{-Aniline})\text{Cr}(\text{CO})_3\text{TS}$) between these two species again using the synchronous transit guided quasi-Newton method. A transition state was located in these calculations as verified by the single low-energy negative eigenvalue (-50 cm^{-1}) of the Hessian matrix. This transition state lies approximately 7 kJ mol^{-1} above the $(\eta^2\text{-}N\text{-Aniline})\text{Cr}(\text{CO})_3$ species. The barrier to the rotation of the $\text{Cr}(\text{CO})_3$ relative to the aniline ligand in $(\eta^2\text{-}N\text{-Aniline})\text{Cr}(\text{CO})_3$ was estimated using a series of relaxed potential energy calculations in which the $\text{Cr}(\text{CO})_3$ fragment was rotated relative to the aniline ligand. The calculated barrier was similar to that obtained for the $(\eta^6\text{-Aniline})\text{Cr}(\text{CO})_3$ complex (12 kJ mol^{-1}) and larger than the energy barrier for the η^2 to η^3 haptropic shift.

The optimized structures of both $(\eta^6\text{-Aniline})\text{Cr}(\text{CO})_3$ and $(\eta^2\text{-}N\text{-Aniline})\text{Cr}(\text{CO})_3$ singlet species were used as starting points for optimisation on the triplet surface. The singlet $(\eta^6\text{-Aniline})\text{Cr}(\text{CO})_3$ species relaxes to a $(\eta^1\text{-C-Aniline})\text{Cr}(\text{CO})_3$ species while the $(\eta^2\text{-}N\text{-Aniline})\text{Cr}(\text{CO})_3$ relaxed to a $(\eta^4\text{-}N\text{-Aniline})\text{Cr}(\text{CO})_3$ species (Fig. 5 (b)). To estimate the relative energies of the optimized structures

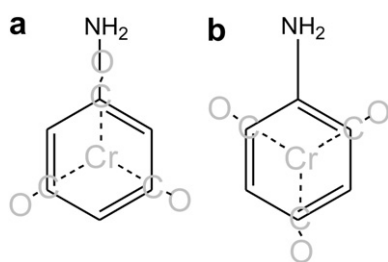


Fig. 7. (a) The eclipsed-*N*-conformation of the optimized $(\eta^6\text{-Aniline})\text{Cr}(\text{CO})_3$ structure. (b) the eclipsed-*C*-conformation obtained in a reaction path modelling calculations (IRC) joining $(\eta^2\text{-}N\text{-Aniline})\text{Cr}(\text{CO})_3$ with $(\eta^6\text{-Aniline})\text{Cr}(\text{CO})_3$.

on both the singlet and triplet surfaces relaxed potential energy scans were performed on both of these surfaces in which the Cr–N distance was reduced from that in $(\eta^6\text{-Aniline})\text{Cr}(\text{CO})_3$ to $(\eta^2\text{-}N\text{-Aniline})\text{Cr}(\text{CO})_3$. Calculation of the energy difference between singlet and triplet species is problematic and consequently we have used the re-parameterized B3LYP* functional in which the exact exchange parameter was set to 0.15 as suggested by Reiher [42,43]. The LANL2DZp basis set was used in these calculations.

The relative energies of the singlet and triplet species for various Cr–N distances are presented in Fig. 8. These results suggest that the energy difference between the singlet and triplet states is smaller for the reduced hapticity species than for $(\eta^6\text{-Aniline})\text{Cr}(\text{CO})_3$. It is important to note that the singlet to triplet energy difference for $(\eta^6\text{-Aniline})\text{Cr}(\text{CO})_3$ in these calculations (approximately 300 kJ mol^{-1}) is similar to a 405 nm photon energy and that those of the reduced hapticity species is considerably less than the photon energy available at 405 nm.

3. Discussion

Previous investigations in our laboratory confirmed that $(\eta^6\text{-Arene})\text{Cr}(\text{CO})_3$ complexes exhibit wavelength dependent photochemistry in low temperature matrixes [26]. In the case of $(\eta^6\text{-Benzene})\text{Cr}(\text{CO})_3$, long wavelength photolysis (450 nm) in a CH_4 matrix at 12 K depleted the bands of $(\eta^6\text{-Benzene})\text{Cr}(\text{CO})_3$ but failed to produce significant product bands apart from uncoordinated CO and a band at 2060 cm^{-1} which was tentatively assigned to a triplet $(\eta^6\text{-Benzene})\text{Cr}(\text{CO})_3$ species. Decreasing the photolysis wavelength to 334 nm was necessary to produce a significant yield of $(\eta^6\text{-Benzene})\text{Cr}(\text{CO})_2$. This is in contrast to the observation of an efficient but slow CO loss following irradiation of $(\eta^6\text{-Benzene})\text{Cr}(\text{CO})_3$ with 400 nm light at room temperature.

In the case of the $(\eta\text{-Aniline})\text{Cr}(\text{CO})_3$ low-temperature matrix studies reported here, the changes observed in the UV/vis. spectrum during the deposition process are explained by the generation of reduced hapticity species, $(\eta^2\text{-}N\text{-Aniline})\text{Cr}(\text{CO})_3$ and $(\eta^3\text{-}N\text{-Aniline})\text{Cr}(\text{CO})_3$. Clearly the calculated energy changes associated with the formation of these species from $(\eta^6\text{-Aniline})\text{Cr}(\text{CO})_3$ is very large compared to that available at 20 K and so it is proposed that relaxation of the distorted CH_4 crystalline matrix surrounding $(\eta^6\text{-Aniline})\text{Cr}(\text{CO})_3$ contributes significantly to the overall Gibbs free energy change which includes the haptotropic shift reaction. At ambient pressures solid CH_4 exists in two phases [44,45]. In phase I, which is stable below 90 K and above 20.4 K, the CH_4 molecules are orientationally disordered, and the crystalline structure can be described as a face centred cubic lattice with the carbon atom at each lattice point and at the centre of a sphere defining the CH_4

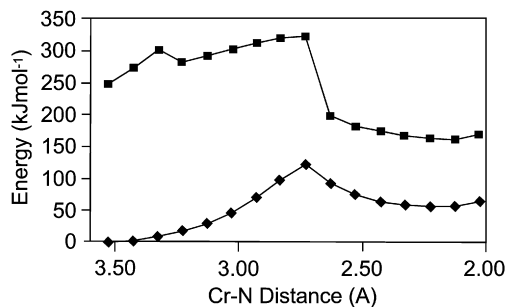


Fig. 8. The relative energies (kJ mol^{-1}) of the singlet and triplet species during the Cr–N relaxed potential energy scan using the B3LYP*/LANL2DZp model chemistry. The energy changes calculated in moving from $(\eta^6\text{-Aniline})\text{Cr}(\text{CO})_3$, (calculated Cr–N distance 3.5273 Å) to $(\eta^3\text{-Aniline})\text{Cr}(\text{CO})_3$ (calculated Cr–N distance 2.1668 Å); ◆ represents the singlet and ■ the triplet surface.

molecular volume. Below 20.4 K (phase II) the CH₄ molecules become partially orientated because of octupole–octupole interactions. The conditions used in the matrix experiments described here suggest that the isolating CH₄ is in phase II during the deposition process and that a phase transition to phase I occurs during the annealing experiments. It is the Gibbs free energy changes associated with this phase change and any associated lattice-defect removal that drives the observed coordination changes.

The nature of the reduced hapticity species are based on IR studies during the deposition process and in subsequent annealing experiments. DFT calculations suggest that these two reduced hapticity species exist as minima on the potential energy hypersurface. They have similar energies and are readily inter-converted over a small energy barrier (6.68 kJ mol⁻¹, Table 4) and their predicted ν_{CO} band positions are close to the observed features (calculated (η³-*N*-Aniline)Cr(CO)₃ 1864, 1875, 1957 cm⁻¹; (η²-*N*-Aniline)Cr(CO)₃ 1867, 1876, 1958 cm⁻¹; observed 1860, 1880, 1962 cm⁻¹). Notwithstanding the small energy barrier between these two reduced hapticity species, the barrier is far in excess of the available thermal energy in the matrix experiments based simply on statistical thermodynamic considerations. The spectral changes presented in Figs. 1 and 2 confirm that while the reduced hapticity species are produced during deposition in a low temperature matrix, raising the temperature of the matrix to 40 K increased their yield and they remained after the matrix was again cooled to 20 K. This suggests that they are not produced by heating the solid (η⁶-Aniline)Cr(CO)₃ as required for the deposition process. The reduced hapticity species absorb further towards the visible region (Fig. 1).

TDDFT calculations on the reduced hapticity species, (η²-*N*-Aniline)Cr(CO)₃ and (η³-*N*-Aniline)Cr(CO)₃, indicate that they absorb at longer wavelength than (η⁶-Aniline)Cr(CO)₃. This means that 405 nm irradiation will preferentially excite the reduced hapticity species over (η⁶-Aniline)Cr(CO)₃. The relative energy of the singlet and triplet species derived from relaxed potential energy scans at the B3LYP*/LANL2DZ level (Fig. 8) show that photolysis of (η⁶-Aniline)Cr(CO)₃ with 405 nm radiation could not populate ³(η⁶-Aniline)Cr(CO)₃ efficiently. However excitation of the reduced hapticity species (η²-*N*-Aniline)Cr(CO)₃ and (η³-*N*-Aniline)Cr(CO)₃ at 405 nm could generate the appropriate triplet species via intersystem crossing from the initially produced singlet excited state.

The single electron vertical excitation energies for ³(η⁴-*N*-Aniline)Cr(CO)₃ were calculated using TDDFT methods. These results (Table 3) indicate that it absorbs across the visible and into the near infrared region of the spectrum. Thus exhaustive irradiations, such as those employed in this study, may result in complete decarbonylation of the triplet metal carbonyl complexes while the triplet character of the resulting metallic fragments inhibits back reaction with photogenerated CO or reaction with active matrix molecules such as N₂. Similar “spin blocking” behaviour was observed in the photochemistry of (η⁵-C₄H₄Se)Cr(CO)₃ reported

Table 4

Relative energies of the complexes in this study. The scale factor derived from the infrared studies (1.018) was applied to the zero point energy correction.

Complex	Energy difference kJ mol ⁻¹ (with respect to complex indicated by column number)			
	1	2	3	4
1. (η ⁶ -Aniline)Cr(CO) ₃				
2. (η ³ - <i>N</i> -Aniline)Cr(CO) ₃	57.2			
3. (η ² - <i>N</i> -Aniline)Cr(CO) ₃	51.4	-5.8		
4. (η ¹ - <i>Cl</i> -Aniline)Cr(CO) ₃ TS	79.1	21.9	27.7	
5. (η ³ - <i>N</i> -Aniline)Cr(CO) ₃ TS	58.1	0.9	6.7	-21.0

previously [46]. It is not possible to determine from these studies if the photo-induced decarbonylation is a concerted process. It is more likely to be a sequential one involving multiple photon absorptions simply on the grounds of the likely M–CO bond strength compared to the available photon energy.

4. Concluding comments

These studies suggest that the low-energy photochemistry of (η-Aniline)Cr(CO)₃ originates from reduced hapticity species (η³-*N*-Aniline)Cr(CO)₃ and (η²-*N*-Aniline)Cr(CO)₃ which are stabilized in low temperature matrixes. Failure to observe intermediate decarbonylated species is explained by the formation of triplet state species which are “spin blocked” to reaction with CO or N₂. Exhaustive steady state photolyses results in complete decarbonylation of the (η-Aniline)Cr(CO)₃ complex. The overall photochemistry of (η⁶-Aniline)Cr(CO)₃ is summarised in the Scheme 1. Further work on the nature of the metallic species produced any potential use of these species in catalytic systems or as small molecule storage devices is currently under investigation.

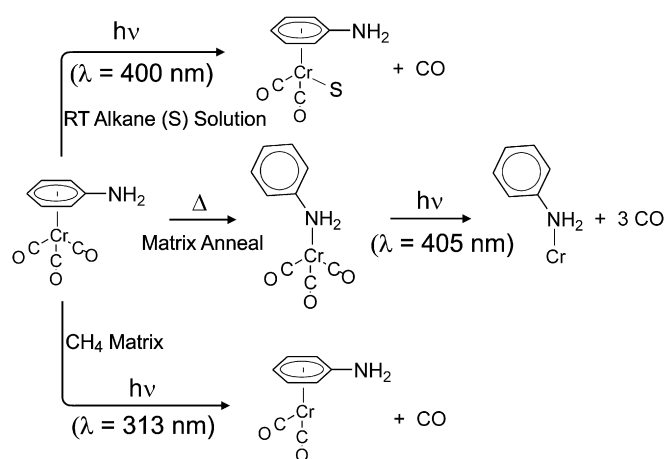
5. Experimental

5.1. Synthesis of (η⁶-Aniline)Cr(CO)₃

This compound was prepared using a slight modification of a published procedure [47,48]. A nitrogen flushed solution of Cr(CO)₆ (0.4 g; 1.8 mmol) and aniline (2.4 g; 24.73 mmol) in dibutylether (12 cm³) and tetrahydrofuran (1 cm³) was brought to its reflux temperature under a nitrogen atmosphere for 24 hours. The resulting yellow solution was filtered through Celite and the solvent removed under reduced pressure. The crude yellow material was purified by vacuum sublimation (ν_{CO} (cyclohexane) 1967, 1893, and 1888 cm⁻¹; (CH₂Cl₂) 1960 and 1876 cm⁻¹).

5.2. Matrix isolation

The Matrix isolation apparatus has been described in elsewhere [49]. Briefly the matrix isolation apparatus consists of a closed cycle helium refrigerator, sample window, shroud, deposition tube, gas mixing chamber, gas inlet, backing pump, diffusion pump and temperature control unit. Matrixes were deposited on a CaF₂ window cooled to 20 K, with matching outer windows on the vacuum shroud. A CS202 closed-cycle refrigerator was used to cool



Scheme 1. The range of photochemical reactions of (η⁶-Aniline)Cr(CO)₃ in both room temperature solution and low temperature matrixes

the sample plate to 20 K, and its temperature was maintained using a Lakeshore 330 autotuning temperature controller. Two stage backing pumps and an oil diffusion pump fitted with a liquid nitrogen trap reduces the shroud pressure to 8×10^{-4} Torr prior to cooling, and achieves better than 10^{-6} Torr when the sample window reaches 20 K. Host gases (Cryo Service) are deposited from the gas mixing chamber via a needle valve connected to two inlet jets positioned either side of the sample tube. A ratio of sample to host matrix in the region 1:2000 was achieved. Typically the rate of gas deposition of 0.3–0.6 Torr/min. provides an appropriate sample-host dilution. Both the sample and isolating gas were deposited simultaneously. The $(\eta^6\text{-Aniline})\text{Cr}(\text{CO})_3$ complex was sublimed from a right angled tube which was electrically heated to 50 °C. The sample deposition was monitored using either UV/vis. or infrared spectroscopy and was stopped when the absorbance of one of the metal carbonyl ν_{CO} bands reached approximately 1 AU. A Perkin–Elmer Spectrum One FTIR spectrophotometer was used to record IR spectra at 1 cm^{-1} resolution from 16 interferograms. A Perkin–Elmer EZ200 double beam scanning spectrophotometer was used to record the UV/vis. spectrum. Matrixes were photolysed using a 200 W Xe/Hg arc lamp in combination with a 10 cm water filter to remove the IR component and appropriate interference filters to select the desired Hg emission line.

5.3. Computational details

DFT methods were used in all calculations presented here. These employed a three parameter hybrid functional (B3) [50], and the Lee–Yang–Parr correlation functional (LYP) i.e. the B3LYP functional. The LANL2DZ and LANL2DZp basis sets were used in the calculations. All calculations were performed using the Gaussian 03 package [51], using HP dual Xeon processor workstations. It is known that the B3LYP functional tends to underestimate the energy of high spin states relative to low spin states [43,52]. Consequently, Reiher has proposed that a reduction in the exact exchange parameter from 0.2 to 0.15 provides a more reliable estimate of the energy difference between spin states in organometallic systems and called this modified functional B3LYP*. For estimates of the energy difference between the singlet and triplet species, the B3LYP* functional was used. These model chemistries represent a compromise between accuracy in measuring energy differences between species with different multiplicities and the computational cost in the large number of optimisation cycles to map the singlet or especially the triplet surfaces. Initial geometries were obtained from molecular mechanics calculations and the final geometries of species located at local energy minima were optimized using tight convergence criteria. Zero point energy corrections were applied to species at stationary points. A listing of internal parameters is provided in the supporting information.

Acknowledgments

CL wishes to thank DCU for the award of a Senior Research Fellowship to support this work.

Appendix. Supplementary data

Supplementary data associated with this article can be found, in the online version, at doi:10.1016/j.jorganchem.2010.04.010.

References

- [1] J.M. Kelly, C. Long, R. Bonneau, *J. Phys. Chem.* 87 (1983) 3344.
- [2] W.R. Peifer, J.F. Garvey, *J. Phys. Chem.* 95 (1991) 1177.

- [3] T.A. Seder, S.P. Church, E. Weitz, *J. Am. Chem. Soc.* 108 (1986) 4721.
- [4] J.D. Simon, X.L. Xie, *J. Phys. Chem.* 93 (1989) 291.
- [5] J.D. Simon, X.L. Xie, *J. Phys. Chem.* 91 (1987) 5538.
- [6] J.D. Simon, X.L. Xie, *J. Phys. Chem.* 90 (1986) 6751.
- [7] J.R. Sprague, S.M. Arrivo, K.G. Spears, *J. Phys. Chem.* 95 (1991) 10528.
- [8] W. Tumas, B. Gitlin, A.M. Rosan, J.T. Yardley, *J. Am. Chem. Soc.* 104 (1982) 55.
- [9] G.W. Tyndall, R.L. Jackson, *J. Chem. Phys.* 89 (1988) 1364.
- [10] X.L. Xie, J.D. Simon, *J. Phys. Chem.* 93 (1989) 4401.
- [11] J.J. Turner, J.K. Burdett, R.N. Perutz, M. Poliakoff, *Pure Appl. Chem.* 49 (1977) 271.
- [12] J.J. Turner, M. Poliakoff, M.B. Simpson, *J. Mol. Struct.* 113 (1984) 359.
- [13] E. Whittle, D.A. Dows, G.C. Pimentel, *J. Chem. Phys.* 22 (1954) 1943.
- [14] S.A. Trushin, W. Fuss, W.E. Schmid, *K.L. Kompa, J. Phys. Chem. A2* (1998) 4129.
- [15] N. Ben Arnor, S. Villaume, D. Maynaud, C. Daniel, *Chem. Phys. Lett.* 421 (2006) 378.
- [16] S. Villaume, A. Strich, C. Daniel, S.A. Perera, R.J. Bartlett, *Phys. Chem. Chem. Phys.* 9 (2007) 6115.
- [17] C. Pollak, A. Rosa, E.J. Baerends, *J. Am. Chem. Soc.* 119 (1997) 7324.
- [18] A. Rosa, E.J. Baerends, S.J.A. van Gisbergen, E. van Lenthe, J.A. Groeneveld, J. G. Snijders, *J. Am. Chem. Soc.* 121 (1999) 10356.
- [19] S.A. Trushin, K. Kosma, W. Fuss, W.E. Schmid, *Chem. Phys.* 347 (2008) 309.
- [20] W. Fuss, S.A. Trushin, W.E. Schmid, *Res. Chem. Intermed.* 27 (2001) 447.
- [21] W. Fuss, W.E. Schmid, S.A. Trushin, *J. Phys. Chem. A* 105 (2001) 333.
- [22] S.A. Trushin, W. Fuss, W.E. Schmid, *Chem. Phys.* 259 (2000) 313.
- [23] W. Fuss, S. Lochbrunner, A.M. Muller, T. Schikarski, W.E. Schmid, S.A. Trushin, *Chem. Phys.* 232 (1998) 161.
- [24] A. Gabrielsson, M. Towrie, S. Zalis, A. Vlcek, *Inorg. Chem.* 47 (2008) 4236.
- [25] M.A.H. Alamiry, N.M. Boyle, C.M. Brookes, M.W. George, C. Long, P. Portius, M. T. Pryce, K.L. Ronayne, X.Z. Sun, M. Towrie, K.Q. Vuong, *Organometallics* 28 (2009) 1461.
- [26] M.A.H. Alamiry, P. Brennan, C. Long, M.T. Pryce, *J. Organomet. Chem.* 693 (2008) 2907.
- [27] T.T. To, E.J. Heilweil, T.J. Burkey, *J. Phys. Chem. A* 110 (2006) 10669.
- [28] T.T. To, E.J. Heilweil, C.B. Duke, K.R. Ruddick, C.E. Webster, T.J. Burkey, *J. Phys. Chem. A* 113 (2009) 2666.
- [29] R. Cohen, E. Weitz, J.M.L. Martin, M.A. Ratner, *Organometallics* 23 (2004) 2315.
- [30] H. Abe, H. Takeo, K.M.T. Yamada, *Chem. Phys. Lett.* 311 (1999) 153.
- [31] PeakFit, Seasolve, 2003.
- [32] C.J. Breheny, S.M. Draper, F.W. Grevels, W.E. Klotzbucher, C. Long, M.T. Pryce, G. Russell, *Organometallics* 15 (1996) 3679.
- [33] J.K. Burdett, M.A. Graham, R.N. Perutz, M. Poliakoff, A.J. Rest, J.J. Turner, R. F. Turner, *J. Am. Chem. Soc.* 97 (1975) 4805.
- [34] J.K. Burdett, J.M. Grzybowski, R.N. Perutz, M. Poliakoff, J.J. Turner, R.F. Turner, *Inorg. Chem.* 17 (1978) 147.
- [35] M.A.H. Alamiry, P. Brennan, A. Coleman, C. Long, M.T. Pryce, *Organometallics* 28 (2009) 94.
- [36] A. Hoellwarth, M. Boehme, S. Dapprich, A.W. Ehlers, A. Gobbi, V. Jonas, K. F. Koehler, R. Stegmann, A. Veldkamp, G. Frenking, *Chem. Phys. Lett.* 208 (1993) 237.
- [37] M.A.H. Alamiry, P. Brennan, C. Long, M.T. Pryce, *J. Organomet. Chem.* 693 (2008) 2907.
- [38] A.A. Low, M.B. Hall, *Int. J. Quantum Chem.* 77 (2000) 152.
- [39] M.J. McGlinchey, *Adv. Organomet. Chem.* 34 (1992) 285.
- [40] O.L. Carter, A.T. McPhail, G.A. Sim, *J. Chem. Soc., Chem. Commun.* (1966) 212.
- [41] O.L. Carter, A.T. McPhail, G.A. Sim, *J. Chem. Soc. a – Inorg. Phys. Theor.* (1967) 228.
- [42] M. Reiher, *Inorg. Chem.* 41 (2002) 6928.
- [43] M. Reiher, O. Salomon, B.A. Hess, *Theor. Chem. Acc* 107 (2001) 48.
- [44] M.A. Neumann, W. Press, C. Noldeke, B. Asmussen, M. Prager, R.M. Ibberson, *J. Chem. Phys.* 119 (2003) 1586.
- [45] M. Hashimoto, M. Hashimoto, T. Isobe, *Bull. Chem. Soc. Jpn* 44 (1971) 2272.
- [46] P. Brennan, M.W. George, O.S. Jina, C. Long, J. McKenna, M.T. Pryce, X.-Z. Sun, Khuong Q. Vuong, *Organometallics* 27 (2008) 3671.
- [47] C.A.L. Mahaffy, J. Hamilton, *Synth. React. Inorg. Met.-Org. Chem.* 17 (1987) 849.
- [48] C.A.L. Mahaffy, P.L. Pauson, *Inorg. Synth* 28 (1990) 136.
- [49] C. Long, K. Maher, M.T. Pryce, *J. Organomet. Chem.* 691 (2006) 3298.
- [50] A.D. Becke, *J. Chem. Phys.* 98 (1993) 5648.
- [51] M.J. Frisch, G.W. Trucks, H.B. Schlegel, G.E. Scuseria, M.A. Robb, J.R. Cheeseman, J.J.A. Montgomery, T. Vreven, K.N. Kudin, J.C. Burant, J.M. Millam, S.S. Iyengar, J. Tomasi, V. Barone, B. Mennucci, M. Cossi, G. Scalmani, N. Rega, G.A. Petersson, H. Nakatsuji, M. Hada, M. Ehara, K. Toyota, R. Fukuda, Y. Hasegawa, M. Ishida, T. Nakajima, Y. Honda, O. Kitao, H. Nakai, M. Klene, X. Li, J.E. Knox, H. P. Hratchian, J.B. Cross, C. Adamo, J. Jaramillo, R. Gomperts, R.E. Stratmann, O. Yazyev, A.J. Austin, R. Cammi, C.J. Pomelli, W. Ochterski, P.Y. Ayala, K. Morokuma, G.A. Voth, P. Salvador, J.J. Dannenberg, V.G. Zakrzewski, S. Dapprich, A. D. Daniels, M.C. Strain, O. Farkas, D.K. Malick, A.D. Rabuck, K. Raghavachari, J.B. Foresman, J.V. Ortiz, Q. Cui, A.G. Baboul, S. Clifford, J. Cioslowski, B.B. Stefanov, G. Liu, A. Liashenko, P. Piskorz, I. Komaromi, R.L. Martin, D.J. Fox, T. Keith, M.A. Al-Laham, C.Y. Peng, A. Nanayakkara, M. Challacombe, P.M.W. Gill, B. Johnson, W. Chen, M.W. Wong, C. Gonzalez, J.A. Pople, *Gaussian 03*, Gaussian, Inc., Wallingford CT, 2004.
- [52] M. Reiher, O. Salomon, D. Sellmann, B.A. Hess, *Chem. a Eur. J.* 7 (2001) 5195.